

## MIT Open Access Articles

*Design and Fabrication of DRIE-Patterned  
Complex Needlelike Silicon Structures*

The MIT Faculty has made this article openly available. **Please share**  
how this access benefits you. Your story matters.

**Citation:** Gassend, Blaise Laurent Patrick, Luis Fernando Velasquez-Garcia, and Akintunde Ibitayo Akinwande. "Design and Fabrication of DRIE-Patterned Complex Needlelike Silicon Structures." *Journal of Microelectromechanical Systems* 19.3 (2010): 589–598. Web. © 2010 IEEE.

**As Published:** <http://dx.doi.org/10.1109/JMEMS.2010.2042680>

**Publisher:** Institute of Electrical and Electronics Engineers

**Persistent URL:** <http://hdl.handle.net/1721.1/70936>

**Version:** Final published version: final published article, as it appeared in a journal, conference proceedings, or other formally published context

**Terms of Use:** Article is made available in accordance with the publisher's policy and may be subject to US copyright law. Please refer to the publisher's site for terms of use.



# Design and Fabrication of DRIE-Patterned Complex Needlelike Silicon Structures

Blaise Laurent Patrick Gassend, Luis Fernando Velásquez-García, *Member, IEEE*, and Akintunde Ibitayo Akinwande, *Fellow, IEEE*

**Abstract**—This paper reports the design and fabrication of high-aspect-ratio needlelike silicon structures that can have complex geometry. The structures are hundreds of micrometers tall with submicrometer-sharp protrusions, and they are fabricated using a series of passivated and unpassivated deep reactive-ion etching (DRIE) steps. A simple model is presented to predict the geometry of the structure based on the etch mask and the etch sequence. Model predictions are in good qualitative agreement with fabrication results, making it a useful design tool. The model is compared with literature reports on tapered DRIE. [2009-0118]

**Index Terms**—Deep reactive-ion etching (DRIE), microneedle, 3-D microfabrication.

## I. INTRODUCTION

THERE are numerous literature reports of microfabrication techniques that produce 3-D features, including wet/dry etching with some degree of isotropy [1], [2], lattice-oriented etching [3], LIGA [4], SU-8 [5], [6], electrochemically welded metallic structures [7], and backside diffuser lithography [8]. Some of these techniques can also produce high-aspect-ratio structures. For silicon, deep reactive-ion etching (DRIE) [9] has proven to be a very versatile fabrication technique that is capable of making high-aspect-ratio structures with high etch rate, straight sidewalls, and small sidewall scalloping [10], [11].

Several researchers have investigated the fabrication of DRIE-patterned structures with nonconstant cross section in the plane that is parallel to the substrate surface. In particular, Roxhed *et al.* reported a tapered version of DRIE [12], where high-aspect-ratio features with sidewalls having up to 36° of

inclination were successfully fabricated. Moreover, Waits *et al.* reported the use of grayscale lithography to produce stratified DRIE-patterned structures [13], [14]. In addition, Li *et al.* studied the use of SF<sub>6</sub>/O<sub>2</sub>-based DRIE to etch tapered holes [15]. Using these approaches, applications such as through-wafer electrical vias [16], [17], Faraday cages [18], and mold tool fabrication [19] have been implemented using DRIE.

There are multiple reports on the fabrication of DRIE-patterned needles, i.e., high-aspect-ratio structures that have sidewalls with nonconstant slope along their heights and that end in sharp protrusions. In particular, both solid [20]–[23] and hollow needles [24] for biological probes and drug delivery, externally fed electrospray emitters [25], [26], and spatially uniform field emitter arrays [27] have been demonstrated. In all these applications, the geometry of the needlelike structures is intimately related to its function. For example, needles for biological probing and drug delivery have a 3-D geometry designed to decrease the trauma to the skin and tissue due to penetration while still providing enough stiffness to avoid structural failure of the needle during insertion [24]. Similarly, needles used as electrospray emitters are hundreds of micrometers tall, are hundreds of micrometers apart, and have submicrometer tip radii so that they can turn on with low voltage [25], [26]. Finally, the needles used as field emitters have nanometer-sharp tips so that they can achieve low turn-on voltage [28]–[30]. Spatially and temporally uniform electron emission from field emitter arrays can be achieved if each emitter is fabricated on top of an individual high-aspect-ratio (100 : 1+) silicon column (the field-emitter-column structure resembles a pencil). The column acts as a current source, effectively limiting the current through each tip [27].

This paper reports the design and fabrication of complex high-aspect-ratio silicon needles. The needlelike structures are fabricated using a sequence of passivated (the standard DRIE process) and unpassivated (no fluorocarbon-based plasma in the process) DRIE steps in combination with an etch mask to achieve a certain geometry, including the generation of ultra-sharp tips. Section II introduces a simple model that predicts the final shape of the structure based on the mask layout and the etch sequence, while Section III compares the fabrication results of test structures with the graphical results from the numerical implementation of the model, and it also compares this paper with literature reports on tapered DRIE.

## II. GEOMETRY MODELING

In this section, a simple model is proposed to predict the needlelike geometry from the mask shape, the duration of the

Manuscript received May 4, 2009; revised October 6, 2009; accepted January 15, 2010. Date of publication March 18, 2010; date of current version June 3, 2010. This work was supported in part by Space and Naval Warfare Systems Center Award N66001-04-1-8925, with Richard Nguyen as the program manager, and in part by U.S. Army Soldiers Systems Command Award W911QY-05-1-0002, with Henry Girolamo as the program manager. Subject Editor R. Ghodssi.

This paper has supplementary downloadable multimedia material available at <http://ieeexplore.ieee.org>, provided by the authors. This material consists of some Matlab code to simulate an alternation of isotropic and anisotropic etches, a .gif file containing a sample mask, and the original C version of the code (total size 10 KB).

B. L. P. Gassend was with the Department of Electrical Engineering and Computer Science, Massachusetts Institute of Technology, Cambridge, MA 02139-4307 USA. He is now with Willow Garage, Menlo Park, CA 94025 USA (e-mail: [gassend@alum.mit.edu](mailto:gassend@alum.mit.edu); [blaise.gassend\\_jmems@m4x.org](mailto:blaise.gassend_jmems@m4x.org)).

L. F. Velásquez-García is with the Microsystems Technology Laboratories, Massachusetts Institute of Technology, Cambridge, MA 02139-4307 USA ([lfvelasq@mit.edu](mailto:lfvelasq@mit.edu); [pegasus@mtl.mit.edu](mailto:pegasus@mtl.mit.edu)).

A. I. Akinwande is with the Department of Electrical Engineering and Computer Science, Massachusetts Institute of Technology, Cambridge, MA 02139-4307 USA (e-mail: [akinwand@mtl.mit.edu](mailto:akinwand@mtl.mit.edu)).

Color versions of one or more of the figures in this paper are available online at <http://ieeexplore.ieee.org>.

Digital Object Identifier 10.1109/JMEMS.2010.2042680

etch steps, and the etch sequence. The etch sequence is composed of unpassivated and passivated DRIE steps. The model does not simulate the dynamics of the interaction between the plasma and the substrate. Instead, each etching step is described by the etch depth and a certain etch profile. The specifics of the model are as follows.

- 1) Each unpassivated DRIE step is modeled as an etch process with an etch rate that is a function only of the normal of the surface being etched. If this function is uniform, the resulting etch is isotropic. However, the bias power of the unpassivated DRIE step produces some anisotropy, making the vertical etch rate higher than the horizontal etch rate.
- 2) For the passivated DRIE steps, the etch proceeds vertically at a uniform rate, except in areas directly below the etch mask, which are assumed unetched by the plasma. This model for the passivated DRIE implies that the bottom of a partially etched wafer remains flat across the full extent of the etch surface. In reality, both chamfers and near-sidewall trenches are common in passivated DRIE and RIE [31].

In addition, the model for the passivated and unpassivated DRIE steps makes no corrections for microloading, scalloping, etch window variation, and any other effect that could reflect in etch nonuniformities across the wafer.

#### A. Model for Passivated and Unpassivated DRIE Steps

The resulting shape after a passivated or an unpassivated DRIE step is complete can be represented by two 2-D functions that vary along the surface of the wafer. In both cases, a first function  $z(x, y)$  defines the depth of the silicon etch at the beginning of the step at each  $(x, y)$  location, where  $x$  and  $y$  are Cartesian coordinates on the wafer surface using a coordinate system with axes in the  $\langle 100 \rangle$  direction (for example, the  $x$ - and  $y$ -axes can be parallel and perpendicular to the wafer flat in a  $\langle 100 \rangle$  wafer, respectively). For the passivated DRIE steps, a second function  $M(x, y)$  defines the areas of the wafer that are protected by an etch mask. Function  $M(x, y)$  only takes on the one or zero value, indicating the presence or absence of masking material, respectively. A passivated DRIE step does not produce undercut, i.e., the etch mask acts as an umbrella that protects the silicon directly below it, even if it is not in direct contact to the etch mask [32]. Therefore, after a passivated DRIE step of depth  $d$ , function  $z$  becomes  $z'$

$$z' = z(x, y) + d \cdot M(x, y). \quad (1)$$

For the unpassivated DRIE steps, a concave shape function  $S(\tilde{x}, \tilde{y})$  is used instead as a second function.  $S$  can take on real values or  $-\infty$  and, for normalization purposes,  $S(0, 0) = 1$ . In general, shape function  $S$  is smooth wherever it is finite. After an unpassivated DRIE step of depth  $d$ , function  $z$  becomes  $z'$

$$z' = \max_{\substack{\tilde{x}, \tilde{y} \\ z(x+d\cdot\tilde{x}, y+d\cdot\tilde{y}) > 0}} [z(x, y), z(x+d\cdot\tilde{x}, y+d\cdot\tilde{y}) + d \cdot S(\tilde{x}, \tilde{y})]. \quad (2)$$

The maximization considers all the positions where the silicon is exposed (i.e., it includes the silicon not directly in contact

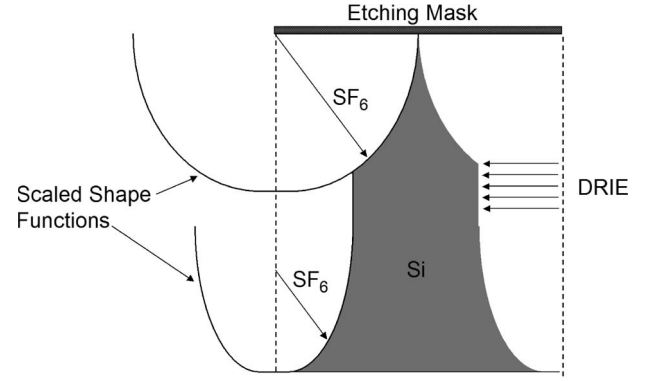


Fig. 1. Geometry of a needlelike structure is generated by scaled shape functions resulting from the unpassivated DRIE steps and by straight sidewalls resulting from the passivated DRIE steps.

with the etch mask) to determine how deep the etch has progressed at a given  $(x, y)$  point. In effect, shape function  $S$  defines the cavity that a hard mask with a point hole in it creates during an unpassivated DRIE step, once the silicon directly below the hole has receded by a unit distance. The model of the unpassivated DRIE step states that the etching proceeds from the exposed silicon surface in all directions, with an etch rate that is a function of the tilt of the sidewall by shape function  $S$ . From the fabrication results, it was concluded that  $S$  defines a roughly ellipsoidal shape with a vertical  $z$ -axis length that is twice the length of any of the in-plane  $x$ - and  $y$ -axes. Also, the model can take into account a slight lattice-orientation-dependent anisotropy in the silicon etch that was experimentally observed. Specifically, the fabrication results suggest that the unpassivated DRIE steps have a small dependence on crystal-plane orientation that causes a slight bulge in the  $x$ - and  $y$ -axes of an ellipsoidal etch, compared to the  $x$ - and  $y$ -axes rotated by  $45^\circ$  with respect to  $\langle 100 \rangle$  (see Section III). In the model, the shape function  $S$  for the unpassivated DRIE steps carried out on a  $\langle 100 \rangle$  wafer is

$$S(x, y) = \sqrt{1 - \beta^2 \cdot (x^2 + y^2) - \alpha \cdot x^2 \cdot y^2} \quad (3)$$

where  $\beta$  is a parameter that describes the directionality of the etch and  $\alpha$  is a parameter that characterizes the lattice-orientation-dependent anisotropy. When the result of (3) is not a real number, it is set to  $S(x, y) = -\infty$ . The constant  $\beta$  was empirically found to vary across the wafer with a typical value of around two. Taking from now on  $\beta = 2$ , empirical results lead to values of  $\alpha$  of about 18.5. For  $\alpha = 0$ , (3) results in an ellipsoid with a  $z$ -axis of length = 1, and  $x$ - and  $y$ -axes of lengths of  $1/\beta$ , i.e., 0.5. The  $x^2 y^2$  term in (3) is the lowest order correction of the symmetry of the etch shape. This correction was sufficient to explain the small anisotropies that were found in the experimental results on  $\langle 100 \rangle$  Si wafers.

The simple model just described can readily be used to determine the final geometry of a silicon structure etched using an arbitrary sequence of passivated and unpassivated DRIE steps. The inputs of the model are the etch mask and the sequence of passivated and unpassivated DRIE steps, including the etch depths of each step. The final shape is an alternation of straight vertical sidewalls and curved inclined surfaces (Fig. 1). The straight vertical sidewalls are generated during the passivated

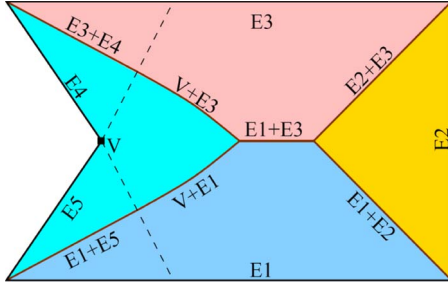


Fig. 2. Etch mask with five straight edges (E1–E5) that has a concave boundary defined by straight edges E4 and E5, which meet at vertex V. The silicon below the mask is etched with an unpassivated DRIE step. The regions determined by the concave stretches of the boundary are shown, as well as the ridges that will result from the interaction of the different mask edges. The dotted lines delimit the area that is controlled by vertex V, the boundaries of which are parabolic.

DRIE steps and are etched inward by subsequent unpassivated DRIE steps. Each unpassivated DRIE step generates a curved inclined surface. The surface for a given unpassivated DRIE step is generated by moving a scaled shape function  $S$  across all points in the silicon surface that are reachable by the plasma at the beginning of the step. Depending on the etch sequence, the surfaces generated during some etch steps will disappear completely as the neighboring surfaces expand and consume them.

### B. Ridge Formation for Ultrasharp Tips

The existence of ridges in an otherwise smooth surface can readily be observed in some of the SEMs shown in Section III, which correspond to the needlelike structures etched with a single unpassivated DRIE step. These discontinuities in the surface normal are predicted by the model. In the opinion of the authors, understanding where the ridges of a needlelike structure appear is essential to produce high-quality ultrasharp tips. According to the model, the ridges occur when control of the etch depth jumps discontinuously from one point to another on the edge of the mask, i.e., where two or more etching fronts meet. Indeed, as shown in Fig. 2, the etch depth of most points below the mask is set by a single point on the edge of the mask. In the figure, each colored region corresponds to points whose depth is set by a given concave stretch of the mask boundary (a stretch in which the border only turns away from the inside of the mask). In each region, the maximum in (2) is reached at exactly one point on the corresponding concave stretch of the boundary. When two regions meet, the maximum is attained in more than one way. In this case, moving slightly away from the boundary causes different mask edges to dominate. The regions dominated by two distant mask edges will not have the same surface normal; therefore, a normal discontinuity is present where these two regions intersect. Likewise, when three regions intersect, a tip is formed.

There are two ideas from computational geometry that are helpful to determine the location of the ridges. These relationships are only exact if  $\alpha$  is zero, i.e., when  $S(x, y)$  has symmetry of revolution. However, the fabrication results demonstrate that the departure from symmetry of revolution in the unpassivated DRIE steps is small enough that it does not have a significant impact on the final shape of the structure. The

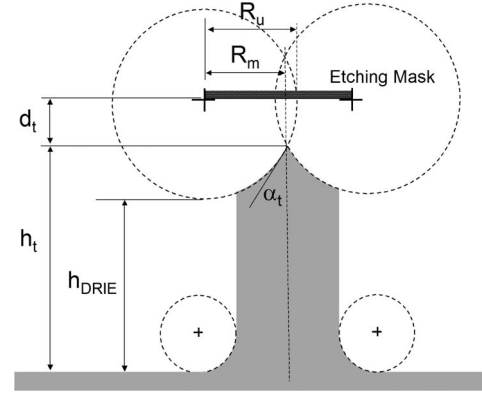


Fig. 3. Needle geometry. The loss of the etch mask during the final unpassivated DRIE step does not affect the applicability of the model.

two ideas are the medial axis transform (MAT) and the distance transform, which are described in the following.

- 1) The MAT of a region is the set of points for which there is more than one closest point on the boundary of the region [33]. For a polygon, the MAT is made up of portions of angular bisectors of edges, perpendicular bisectors of vertices, and parabolas that have one edge as a directrix and one vertex as a focus. The MAT of the etch mask defines the projection of the ridges on the etch mask surface. The MAT can easily be sketched by hand and is an excellent aid in designing mask shapes for microneedles.
- 2) The distance transform of a mask shape is a function  $DT(x, y)$  that maps each point in the plane to the distance from that point to the closest point outside the mask. This function is zero in areas not covered by the mask and steadily increases inside the mask [34]. Equation (2) is closely related to the definition of the distance transform, so that the final shape of the needlelike structure can be expressed by

$$z(x, y) = f(DT(x, y)) \quad (4)$$

where  $f$  is a function that depends on the sequence of etches that was performed. The ridges arise because  $DT(x, y)$  is not smooth on the MAT.

So far, only needlelike structures formed from a single unpassivated DRIE step have been discussed. Another type of ridge appears when a passivated DRIE step is part of the sequence because the passivated DRIE steps introduce discontinuities in  $f$ . These discontinuities lead to discontinuities in  $z(x, y)$ , with an edge at the top of the corresponding vertical DRIE sidewalls.

### C. Needle Geometry and Uniformity

The presented model allows the detailed prediction of the geometry of a DRIE-etched structure. However, early in the design process, it is often more useful to have a reduced-order analytical model to compute basic structure parameters. In this section, it is shown how to estimate for a needlelike structure the tip half-angle  $\alpha_t$ , tip height  $h_t$ , and tip depth  $d_t$  from the mask radius  $R_m$ , the passivated DRIE etch depth  $h_{DRIE}$ , and the amount of undercut  $R_u$  (Fig. 3) if the sequence that is used consists of an unpassivated DRIE step, followed by a



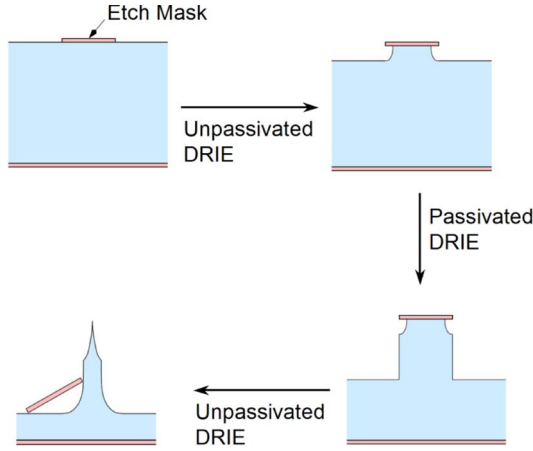


Fig. 4. Base DRIE sequence to fabricate needlelike structures.

passivated DRIE step and, finally, an unpassivated DRIE step (Fig. 4). An unpassivated–passivated–unpassivated DRIE step sequence is the basic sequence to make microscaled [35] and mesoscaled [25] solid needles. The tip half-angle  $\alpha_t$  is the angle between the vertical direction and the steepest surface arriving at the tip. The tip height  $h_t$  is the height of the tip above the lowest etched level. The tip depth  $d_t$  is the distance between the tip and an unetched silicon surface (the top of the wafer). The mask radius  $R_m$  is the horizontal distance from the tip to the edge of the mask, which, for a mask yielding a single needle with only one tip, is the radius of the largest inscribed circle for the mask. The passivated DRIE etch depth  $h_{\text{DRIE}}$  is the total vertical distance etched by the passivated DRIE step. The amount of undercutting  $R_u$  is the distance etched inward during the different unpassivated DRIE steps. The expressions that describe the structure shown in Fig. 3 are

$$d_t = k \cdot \sqrt{R_u^2 - R_m^2} \quad (5)$$

$$h_t = h_{\text{DRIE}} + k \cdot \left( R_u - \sqrt{R_u^2 - R_m^2} \right) \quad (6)$$

$$\tan(\alpha_t) = \frac{1}{k} \cdot \sqrt{\left( \frac{R_u}{R_m} \right)^2 - 1}. \quad (7)$$

Equations (5)–(7) come directly from simple geometry, and they assume that the unpassivated DRIE steps are described by a shape function that is an ellipsoid with a vertical dimension that is  $k$  times greater than the horizontal dimensions (from the fabrication results,  $k$  is about two). Also, the equations assume that a tip is actually formed, i.e.,  $R_u > R_m$ . Moreover, the equations assume that no passivated DRIE etching takes place after the mask has fallen off.

Equations (5)–(7) can be rearranged to give the undercut that is needed to achieve a particular half-angle, as well as the depth at the tip-to-total height ratio for that half-angle

$$d_t = k^2 \cdot R_m \cdot \tan(\alpha_t) \quad (8)$$

$$R_u = R_m \cdot \sqrt{k^2 \cdot \tan^2(\alpha_t) + 1} \quad (9)$$

$$\frac{h_t}{h_t + d_t} = 1 - \frac{1}{\sqrt{1 + \frac{1}{k^2 \cdot \tan^2(\alpha_t)}}}, \quad \text{when } h_{\text{DRIE}} = 0. \quad (10)$$

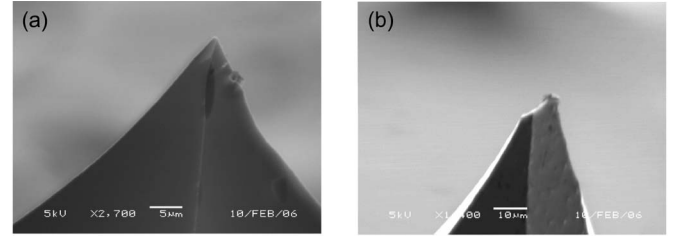


Fig. 5. (a) Sharp silicon tip formed when three etch fronts meet and (b) a bladelike tip formed when four etch fronts meet.

In practice, it was found that  $h_{\text{DRIE}}$  is uniform to within 10%, but  $R_u$  and  $k$  were observed to vary across the wafer by as much as 50%, mainly due to systematic radial etch nonuniformity. The spatial nonuniformity limits the quantitative global prediction power of the model. Equations (8)–(10) have infinite derivatives as  $R_u$  approaches  $R_m$ . Therefore, to reduce sensitivity to process variation in a needle batch fabrication, it is preferable to overetch to some extent so that tips with comparable sharpness and height are formed for all the needles in the array. In designing the microneedle geometry, this sensitivity needs to be traded off with the fact that as  $R_u$  increases, the tip half-angle and depth  $d_t$  also increase, while height  $h_t$  decreases. If tall needles with good height uniformity are desired, the best option is to use a small etch mask. Using this approach, the height of the needles will mainly be set by  $h_{\text{DRIE}}$ , as the value of  $R_u$  can be kept small. The risk with thin tall needles is that they may be undercut if the passivated DRIE has a negative taper. To circumvent this problem, the first unpassivated DRIE step can be increased, or the passivated DRIE recipe can be tuned so that it does not have negative sidewalls for the mask layout used in making the needles.

The fabrication results show that DRIE-patterned sharp tips can only be reliably obtained if the tip is formed at the meeting point of only three ridges [Fig. 5(a)]. If one of the ridges is shifted because the etch is progressing at a different rate compared to the other two ridges, the position of the tip is moved slightly, but the tip remains sharp. This is unlike the case where four or more ridges are involved in the formation of the tip, in which the tip can become a straight edge [Fig. 5(b)]. Moreover, the three ridges should ideally meet at  $120^\circ$  from each other so that the tip is symmetric. The tips can be further sharpened by implementing a series of thermal oxide growth and removal steps, as several researchers have shown [20], [30], [35].

The fabrication results also show that, sometimes, the tip of the needle looks fractured (Fig. 6) instead of forming a clean sharp point. The authors speculate that the tip fracture is caused by the falling of the etch mask before the final unpassivated DRIE step is completed. In the ideal case, the hard mask falls off when the needle tip is sharpened by the convergence of unpassivated DRIE etch fronts. In practice, it is possible for the etch mask to transmit a load (force and/or torque) that causes the tip to break slightly before the sharp tip formation occurs, thus resulting in a fractured tip. For example, this break could take place when the substrate is removed from the DRIE tool to examine the etch progress. Fractured tips are usually duller than fully sharpened tips. However, it is still possible to produce sharp tips from broken tips by overetching the needles using an

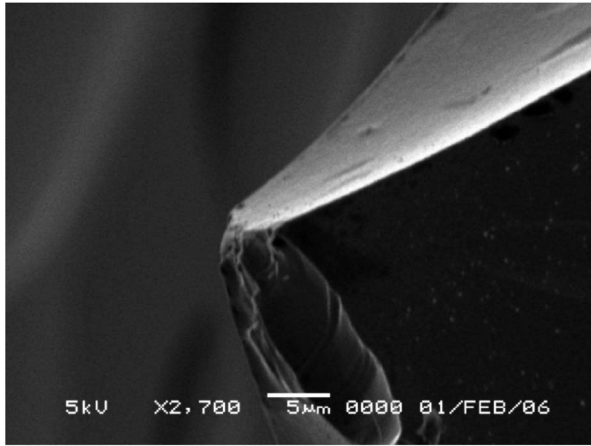


Fig. 6. Needlelike structure with a broken tip.

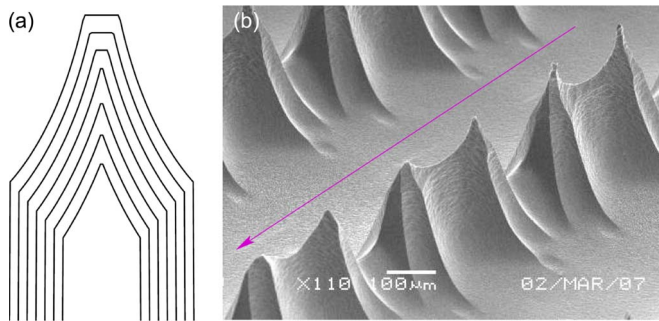


Fig. 7. (a) Numerical simulation of the sharpening of a broken needle tip using an unpassivated DRIE step and (b) a series of tips with overetch increasing in the direction of the arrow.

unpassivated DRIE step (Fig. 7). Another possible approach to avoid tip fracture is to remove the free-hanging part of the etch mask before it breaks off (oxygen plasma for a photoresist etch mask and HF vapors for an oxide etch mask) and then to slightly overetch using an unpassivated DRIE step. The removal of the free-hanging part of the etch mask makes it less likely for the tip to break due to pressure-induced loads.

### III. MODEL COMPARISON WITH FABRICATED STRUCTURES, TAPERED DRIE

This section provides a qualitative evaluation of the model, i.e., an evaluation of the visual resemblance of the etched structures to the predictions of the model. No point-to-point quantitative comparison of the model was attempted. Because of the large radial nonuniformity of the etch that was observed, a quantitative comparison would require the use of etch depths and shape functions that depend on the position on the wafer. Also, this section illustrates how the model presented in this paper is related to the reported work on tapered DRIE, particularly the work of Roxhed *et al.* [12]. All the experimental results in this section come from  $\langle 100 \rangle$  silicon wafers.

#### A. Anisotropy Calibration

The fabrication result shown in Fig. 8 was used to calibrate the amount of lattice-orientation-dependent anisotropy of the unpassivated DRIE etch in the model [ $\alpha$  in (3)]. Fig. 8(a)

shows a top view of a conical needle created using an eight-tip star as an etch mask. The eight points of the star produce visible ridges going across the sides of the structure. The edge anisotropy causes the ridges to deviate slightly so that the ridges are paired before reaching the tip of the etch structure. Each pair of cojoined ridges merges into a single ridge that continues straight up to the tip of the structure. Fig. 8(b) shows the same behavior when lattice-orientation-dependent anisotropy is added to the etch model ( $\alpha = 18.5$ ). Unfortunately, with the unpassivated DRIE recipes used in the fabrication of the test structures, the amount of anisotropy varies across the wafer, preventing quantitative validation of the model. It is speculated the factors such as microloading, wafer temperature nonuniformities due to nonideal wafer handler mounting, and local plasma composition nonuniformities influence the lattice-orientation-dependent etch anisotropy uniformity.

#### B. Basic Needles

Fig. 9 shows various microneedle geometries made using the base process flow shown in Fig. 4. The needles shown are 300–400  $\mu\text{m}$  tall. The pencil-like needle [Fig. 9(a)] was fabricated using an 8-point star with 100- $\mu\text{m}$  ID and 200- $\mu\text{m}$  OD as an etch mask, and it required 50  $\mu\text{m}$  of underetching before its cap (etch mask) detached, as well as 300  $\mu\text{m}$  of passivated DRIE etching. The conical needle [Fig. 9(b)] uses the same mask shape as the pencil-like needle, scaled-up four times (the etch mask is an eight-point star with 400- $\mu\text{m}$  ID and 800- $\mu\text{m}$  OD). This type of needle requires 200  $\mu\text{m}$  of underetching and no passivated DRIE etching at all. The mask for the needle with a serrated top edge [Fig. 9(c)] is a rectangle that is 130  $\mu\text{m}$  wide with periodic triangular outcroppings (teeth) separated 100  $\mu\text{m}$  along the direction of the ridge. The tooth angle is  $45^\circ$ , i.e., there is a right angle of the mask at the end of each tooth. This type of needle requires 50  $\mu\text{m}$  of underetching. The model correctly predicts the position of the tips. However, the graphical result of the model shows the tips rising above the rest of the needle edge more than in the SEMs, and it also misses the slight curvature of the ridge between adjacent tips. The disagreement between the tip height predicted by the model and the experimental result might be due to slight overetching of the sample. Moreover, the model does not account for a partial shadowing effect caused by the mask that is stronger when the etch front is closer to the points of contact between the mask and the substrate (i.e., the tips). This effect is similar to microloading [36] but inherently related to etches with isotropy. The partial shadowing will cause progressively more material to be removed farther from the tips and, hence, the curvature that is observed in the SEM. The model is unable to capture this effect as it only considers shadowing from the nearest mask edge to any given point. Thus, the model incorrectly predicts that the ridge should be flat more than one mask-tooth half-length away from the tip.

#### C. Complex Needles

The range of needle structures that can be produced could be extended if the base sequence shown in Fig. 4 is modified by the addition of extra steps. The results shown in this section use three unpassivated DRIE steps interleaved with two passivated

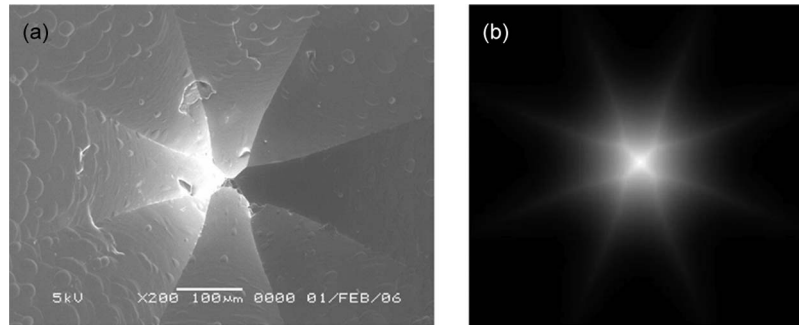


Fig. 8. (a) Top view of a mountainlike needle showing etching anisotropy and (b) graphical result of the model tuned to reproduce the anisotropy effect.

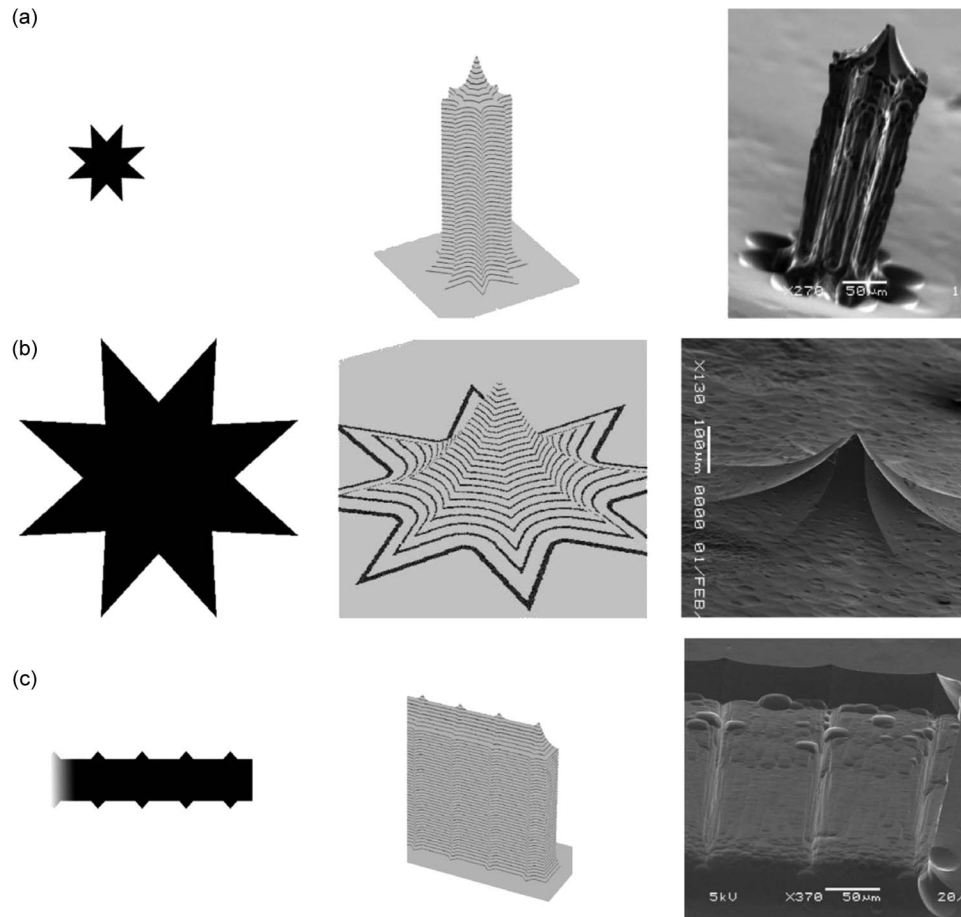


Fig. 9. (Left) Mask, (center) graphical model prediction, (right) and fabrication result of (a) a pencil-like needle, (b) a conic needle, and (c) a needle with a serrated top edge.

DRIE steps, which is also the etch sequence that was used by Roxhed *et al.* to fabricate ultrasharp microneedles for drug delivery [24]. Fig. 10 shows the clear resemblance between the model predictions and fabrication results for two different etch masks. In Fig. 10(a), the full width of the mask is  $340\text{ }\mu\text{m}$ , while in Fig. 10(b), the whole shape is inscribed in a circle of  $400\text{-}\mu\text{m}$  radius. The most striking discrepancy between the model and the fabricated result is in Fig. 10(a), where the sharp vertical ridges predicted at the tips of the starlike structure were largely eroded away in the sample, to the point where the SEM shows a convex ridge line where the model predicted a concave ridge line with a sharp corner. This discrepancy is most likely due to the sharpness of the star's points. First, any small amount of overetching will significantly move the ridge line. Second,

the sharp corner predicted by the model is likely to enhance the local electric field, which will lead to an increase of ion bombardment and excessive etching. Finally, the sample shown in Fig. 10(a) was slightly overetched compared to the model, reducing how much the central part of the tip extends above the star shape.

In one of the test structures [swirl needle, Fig. 10(b)], capillarylike features were etched into the needle in an attempt to increase the flow rate that could be delivered by the structure, compared to the flow rate that the needle would deliver if it were coated by a surface wicking material such as black silicon [25], [37]. The fabrication results are similar to that obtained by other researchers with grayscale lithography and passivated DRIE [13], [14]. However, the slope transitions are smoother.



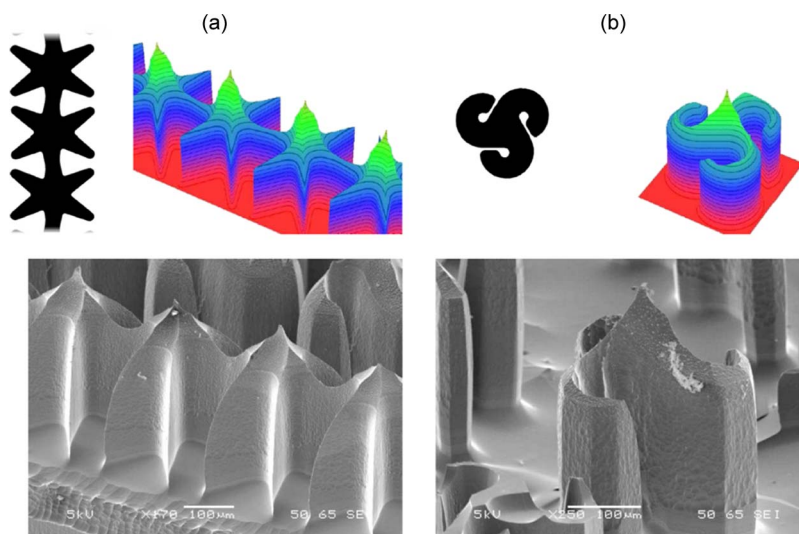


Fig. 10. (Top left) Mask, (top right) graphical model prediction, and (bottom) fabrication result for (a) a tightly packed row of star-shaped needles and (b) a swirl needle.

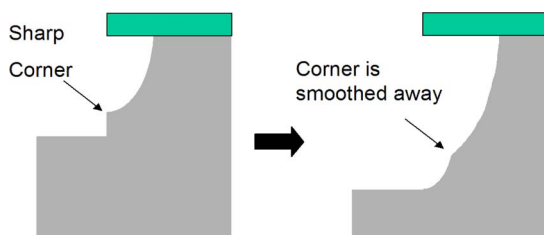


Fig. 11. (Left) Sharp corner is visibly smoothened by (right) a long-enough unpassivated DRIE step.

#### D. Tapered DRIE

Roxhed *et al.* reported a model for the tapered DRIE that satisfactorily predicts the fabrication results over a range of processing parameters [12]. The model proposed by Roxhed *et al.* states that the etch profile of a sequence of unpassivated and passivated DRIE steps with arbitrary duration is a straight line. However, several fabrication results shown in [12] clearly deviate from this approximation. In particular, the top of the etch profile near the etch mask is concave, and in some cases, the tapered etch profile does not resemble a straight line but a staggered line with a more or less straight envelope. The authors of this paper would like to illustrate how the model proposed by Roxhed *et al.* to describe the tapered DRIE is a special case of the model described in this paper. First, consider an etched structure made by an unpassivated DRIE step, followed by a short passivated DRIE step (Fig. 11). The result is a vertical sidewall that ends in a sharp corner at the point where the passivated DRIE etch profile meets the unpassivated DRIE etch profile. If the etch sequence is followed by a sufficiently long unpassivated DRIE step, the sharp corner is etched away. Now, consider the set of circles shown in Fig. 12. The centers of the circles are aligned and equally spaced out. The radius of the circle decreases by a constant amount when moving from one circle to the next. The envelope of these circles is a straight line. Using this reasoning, if the passivated and unpassivated DRIE steps are alternated in short sequences, the resulting sidewall is the envelope of a set of ellipsoids, which is an inclined straight line. In principle, any taper could be obtained with this method by varying the proportion of the total etch made by all

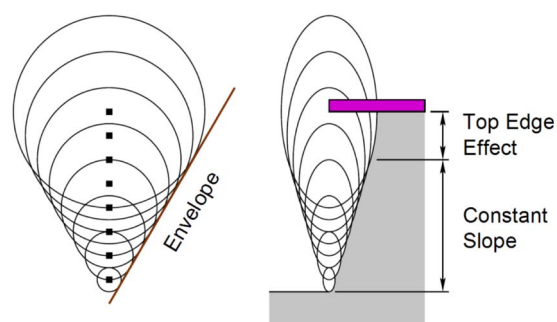


Fig. 12. (Left) The envelope of a set of evenly spaced circles defines a straight line. (Right) Using this reasoning, a set of tightly spaced passivated and unpassivated DRIE steps defines an etch profile with constant slope, except at the top of the profile.

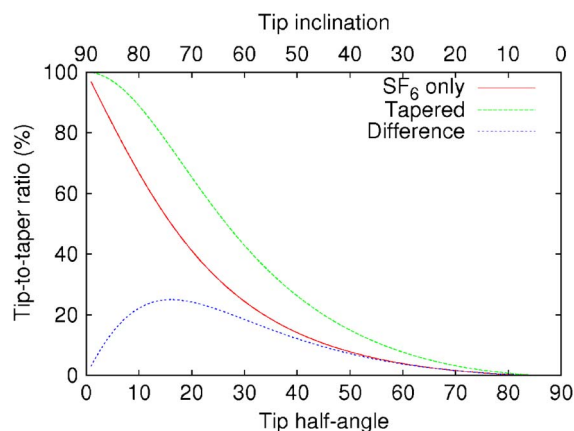


Fig. 13. Comparison of the tip-to-total depth ratio for a needle etched with unpassivated DRIE only ( $\text{SF}_6$ ) and a needle etched with constant taper when  $k=2$ .

the unpassivated and passivated DRIE steps as compared to the total etch depth. As expected, a constant taper is obtained only if short unpassivated and passivated DRIE steps are alternated. It is clear in Fig. 12 that the top edge of the etch profile is not straight. The top of the etch profile is set by the largest ellipsoid, which results in having a chamfer on the sidewall next to the etch mask. Because of this chamfer, there is a practical limit to how far from vertical the tapered sidewall can be. As



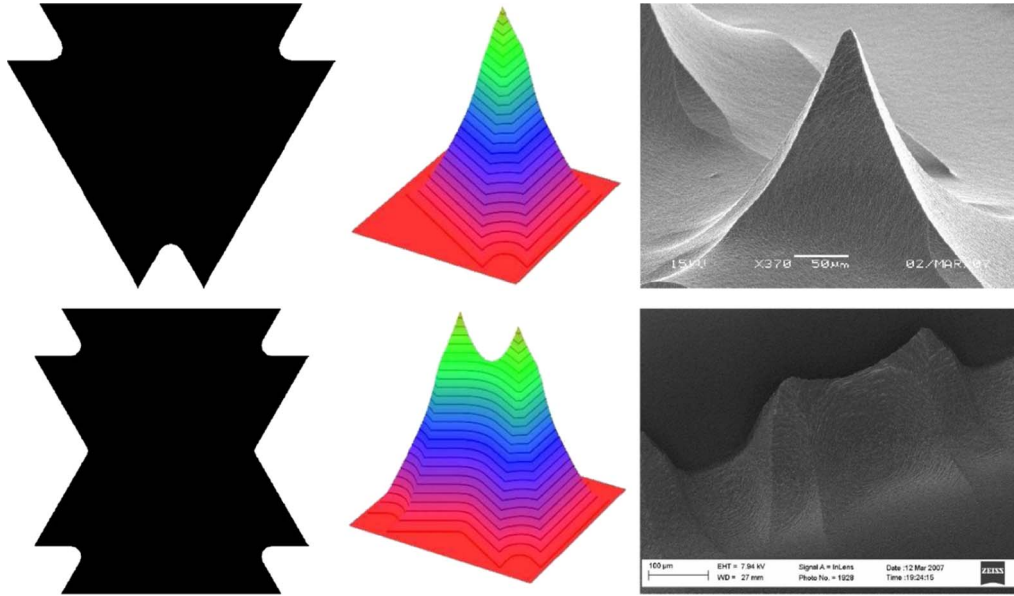


Fig. 14. (Left) Etch mask, (center) predicted result by the model, and (right) fabrication result of the microfabricated (top) one- and (bottom) two-pointed needles with constant taper.

the sidewall becomes shallower and shallower, the “top edge effect” from Fig. 12 becomes the dominant part of the structure, limiting practical sidewall angles to at most  $30^\circ$ – $45^\circ$  from vertical. The bottom of the etch profile is defined by the smallest ellipsoid, which, in principle, can be set arbitrarily small. These features are confirmed by the experimental results of Roxhed *et al.*, except the negative taper that they observe at the top of the sidewall. It is important to point out that the passivated DRIE is, in itself, a tight series of etching and polymer-coating steps, where the processing conditions are tuned so that an etch step gets through the polymer coating deposited at the bottom of the trench, but not through the sidewall coating, thus resulting in vertical sidewall formation.

The fact that constant taper sidewalls can be obtained using an alternation of short passivated and unpassivated DRIE steps can be applied to the fabrication of needles. In particular, the sidewall of the needle can have the same slope as the needle tip. Under these circumstances, because the top of the etched profile is set by the largest ellipsoid, the top of the profile will have to be etched away, increasing the tip depth. Equation (8) gives the tip depth, and for a tapered needle, the tip height satisfies  $h_t \cdot \tan[\alpha_t] = R_m$ . Thus, the tip-to-total height ratio in the case of a needle with constant tapered sidewalls becomes

$$\frac{h_t}{h_t + d_t} = \frac{1}{1 + k^2 \cdot \tan(\alpha_t)}. \quad (11)$$

The use of constant taper in needles results in an improvement in the percentage of utilization of the total etch depth  $h_t + d_t$ . Fig. 13 compares (10) (only unpassivated DRIE is performed) with (11). For example, the tapered etch has a tip-to-total depth ratio of 65% at  $20^\circ$ , while the same ratio for the case of unpassivated DRIE only is 41%.

Tapered sidewalls can also be implemented without the need of a series of passivated and unpassivated DRIE steps. In this case, we use the fact that the passivated DRIE is already an alternation of passivation and etching steps. For example, a standard passivated DRIE recipe can be modified by shortening

TABLE I  
PARAMETERS TO ACHIEVE  $70^\circ$  TAPERED SIDEWALLS (BGJBMOD)  
COMPARED TO THE ORIGINAL PARAMETERS TO ACHIEVE  
STRAIGHT WALLS (JBETCH)

Parameter	BGJBMOD		JBETCH	
Pressure	28		28	
	Etch	Passivate	Etch	Passivate
Duration	30	1.9	13	11
C <sub>4</sub> F <sub>8</sub>	0	35	0	50
SF <sub>6</sub> Flow	105	0	105	0
Coil	800	600	800	600
Platen	5	6	15	6

its passivation step and by increasing the duration of its etch step so that the sidewall passivation runs out before the end of the etch step, making it possible to achieve the same result of a long series composed of a single passivated DRIE cycle, followed by a short unpassivated DRIE step. Using this reasoning, one of the DRIE recipes used in the MIT microengine project to etch the long and narrow journal bearing of the turbomachinery [38] was modified to fabricate needles with  $70^\circ$  sidewalls (Fig. 14). The process parameters of both recipes are provided in Table I.

#### IV. CONCLUSION

The design and fabrication of complex high-aspect-ratio needlelike structures have been reported. The structures are fabricated using a series of passivated and unpassivated DRIE steps. A simple model has been proposed to design complex needlelike silicon structures based on the etch mask and the etch sequence. The model has good qualitative agreement with the fabrication results. However, etch uniformity, photolithography uniformity, and lattice-orientation-dependent etch anisotropy prevent accurate quantitative prediction of the shape. Connections between the formation of ridges and two computational

geometry primitives have been highlighted. A reduced-order model has been provided to obtain analytical understanding of the geometry of a needle, given an etch mask and a base process flow of unpassivated–passivated–unpassivated DRIE steps. The model has been compared to the reported literature on tapered DRIE, and it has been found to successfully predict the formation of needles with straight tapered sidewalls. The model is useful for designing needles for diverse applications such as biological probes, field emission, and electrospray.

#### ACKNOWLEDGMENT

The authors would like to thank the Microsystems Technology Laboratories (MTL) staff for their invaluable support. The needle structures were fabricated using the MIT MTL facilities.

#### REFERENCES

- [1] W. A. Kern, "Chemical etching," in *Thin Film Processing*, J. L. Vossen, Ed. New York: Academic, 1978.
- [2] D. M. Manos and D. L. Flam, Eds., *Plasma Etching: An Introduction*. Boston, MA: Academic, 1989.
- [3] W. Kern, "Chemical etching of silicon, germanium, gallium arsenide, and gallium phosphide," *RCA Rev.*, vol. 39, pp. 278–308, Jun. 1978.
- [4] IMM Institut für Mikrotechnik GmbH, H. Lehr, The LIGA Technique (Commercial Brochure), Mainz-Hetchsheim, Germany 1995.
- [5] R. Angelo, J. D. Gelorme, J. P. Kuczynski, W. H. Lawrence, S. P. Pappas, and L. L. Simpson, "Photocurable epoxy composition with sulfonium salt photoinitiator," U.S. Patent 5 102 772, Apr. 7, 1992.
- [6] A. Bertsch, H. Lorenz, and P. Renaud, "3D microfabrication by combining microstereolithography and thick resist UV photolithography," *Sens. Actuators A, Phys.*, vol. 73, no. 1/2, pp. 14–23, Mar. 1999.
- [7] R. J. Jackman, S. T. Brittain, and G. M. Whitesides, "Fabrication of three-dimensional microstructures by electrochemically welding structures formed by microcontact printing on planar and curved substrates," *J. Microelectromech. Syst.*, vol. 7, no. 2, pp. 261–266, Jun. 1998.
- [8] J.-H. Lee, W.-S. Choi, K.-H. Lee, and J.-B. Yoon, "A simple and effective fabrication method for various 3D microstructures: Backside 3D diffuser lithography," *J. Micromech. Microeng.*, vol. 18, no. 12, p. 125015, Nov. 2008.
- [9] F. Lärmer and A. Schilp, "Method of anisotropically etching silicon," U.S. Patent 5 501 893, Mar. 26, 1996.
- [10] A. A. Ayon, R. Braff, C. C. Lin, H. H. Sawin, and M. A. Schmidt, "Characterization of a time multiplexed inductively coupled plasma etcher," *J. Electrochem. Soc.*, vol. 146, no. 1, pp. 339–349, Jan. 1999.
- [11] K.-S. Chen, A. Ayon, X. Zhang, and S. Spearing, "Effect of process parameters on the surface morphology and mechanical performance of silicon structures after deep reactive ion etching (DRIE)," *J. Microelectromech. Syst.*, vol. 11, no. 3, pp. 264–275, Jun. 2002.
- [12] N. Roxhed, P. Griss, and G. Stemme, "Tapered deep reactive ion etching: Method and characterization," in *Proc. 14th IEEE Int. Conf. Solid-State Sens., Actuators, Microsyst.*, Lyon, France, Jun. 10–14, 2007, pp. 493–496.
- [13] C. M. Waits, B. Morgan, M. Kastantin, and R. Ghodssi, "Microfabrication of 3D silicon MEMS structures using gray-scale lithography and deep reactive ion etching," *Sens. Actuators A, Phys.*, vol. 119, no. 1, pp. 245–253, Mar. 2005.
- [14] C. M. Waits, A. Modafe, and R. Ghodssi, "Investigation of gray-scale technology for large area 3D silicon MEMS structures," *J. Micromech. Microeng.*, vol. 13, no. 2, pp. 170–177, Dec. 2003.
- [15] R. Li, Y. Lamy, W. F. A. Besling, F. Roozeboom, and P. M. Sarro, "Continuous deep reactive ion etching of tapered via holes for three-dimensional integration," *J. Micromech. Microeng.*, vol. 18, no. 2, p. 125023, Dec. 2008.
- [16] R. Nagarajan, L. Ebin, L. Dayong, S. C. Seng, K. Prasad, and N. Balasubramanian, "Development of a novel deep silicon tapered via etch process for through-silicon interconnection in 3-D integrated systems," in *Proc. 56th Electron. Compon. Technol. Conf.*, San Diego, CA, 2006, pp. 383–387.
- [17] J. H. Wu, J. Scholvin, and J. A. del Alamo, "A through-wafer interconnect in silicon for RFICs," *IEEE Trans. Electron Devices*, vol. 51, no. 11, pp. 1765–1771, Nov. 2004.
- [18] J. H. Wu, J. Scholvin, J. A. del Alamo, and K. A. Jenkins, "A Faraday cage isolation structure for substrate crosstalk suppression," *IEEE Microw. Wireless Compon. Lett.*, vol. 11, no. 10, pp. 410–412, Oct. 2001.
- [19] S.-B. Jo, M.-W. Lee, S.-G. Lee, E.-H. Lee, S.-G. Park, and B.-H. O, "Characterization of a modified Bosch-type process for silicon mold fabrication," *J. Vac. Sci. Technol. A, Vac. Surf. Films*, vol. 23, no. 4, pp. 905–910, 2005.
- [20] Y. Hanein, C. G. J. Schabmueller, G. Holman, P. Lucke, D. D. Denton, and K. F. Böhringer, "High-aspect ratio submicrometer needles for intracellular applications," *J. Micromech. Microeng.*, vol. 13, no. 4, pp. S91–S95, Jun. 2003.
- [21] M. Schuettler, S. Stiess, B. V. King, and G. J. Suaning, "Fabrication of implantable microelectrode arrays by laser cutting of silicone rubber and platinum foil," *J. Neural Eng.*, vol. 2, no. 1, pp. S121–S128, Feb. 2005.
- [22] W. Cunningham, K. Mathieson, F. A. McEwan, A. Blue, R. McGeachy, J. A. McLeod, C. Morris-Ellis, V. O'Shea, K. M. Smith, A. Litke, and M. Rahman, "Fabrication of microelectrode arrays for neural measurements from retinal tissue," *J. Phys. D, Appl. Phys.*, vol. 34, no. 18, pp. 2804–2809, Sep. 2001.
- [23] K. Mathieson, S. Kachiguine, C. Adams, W. Cunningham, D. Gunning, V. O'Shea, K. M. Smith, E. J. Chichilnisky, A. M. Litke, A. Sher, and M. Rahman, "Large-area microelectrode arrays for recording of neural signals," *IEEE Trans. Nucl. Sci.*, vol. 51, no. 5, pp. 2027–2031, Oct. 2004.
- [24] N. Roxhed, T. C. Gasser, P. Griss, G. A. Holzapfel, and G. Stemme, "Penetration-enhanced ultrasharp microneedles and prediction on skin interaction for efficient transdermal drug delivery," *J. Microelectromech. Syst.*, vol. 16, no. 6, pp. 1429–1440, Dec. 2007.
- [25] L. F. Velásquez-García, A. I. Akinwande, and M. Martinez-Sanchez, "A planar array of micro-fabricated electrospray emitters for thruster applications," *J. Microelectromech. Syst.*, vol. 15, no. 5, pp. 1272–1280, Oct. 2006.
- [26] B. Gassend, L. F. Velásquez-García, A. I. Akinwande, and M. Martinez-Sanchez, "A microfabricated planar electrospray array ionic liquid ion source with integrated extractor," *J. Microelectromech. Syst.*, vol. 18, no. 3, pp. 679–694, Jun. 2009.
- [27] L. F. Velásquez-García, B. Adeoti, Y. Niu, and A. I. Akinwande, "Uniform high current field emission of electrons from Si and CNF FEAs individually controlled by Si pillar ungated FETs," in *IEDM Tech. Dig.*, Washington, DC, 2007, pp. 599–602.
- [28] H. H. Busta, B. J. Zimmerman, M. C. Tringides, and C. A. Spindt, "DC I–V characteristics of field emitter triodes," *IEEE Trans. Electron Devices*, vol. 38, no. 11, pp. 2558–2562, Nov. 1991.
- [29] R. M. Mobley and J. E. Boers, "Computer simulation of micro-triode performance," *IEEE Trans. Electron Devices*, vol. 38, no. 10, pp. 2383–2388, Oct. 1991.
- [30] M. Ding, G. Sha, and A. I. Akinwande, "Silicon field emission arrays with atomically sharp tips: Turn-on voltage and the effect of tip radius distribution," *IEEE Trans. Electron Devices*, vol. 49, no. 12, pp. 2333–2342, Dec. 2002.
- [31] I. W. Rangelow, P. Thoren, and R. Kassing, "Computer simulation of pattern profiles through physical etching with shadow, trenching, and redeposition," *Microelectron. Eng.*, vol. 3, no. 1–4, pp. 631–638, Dec. 1985.
- [32] L. F. Velásquez-García, "The design, fabrication and testing of microfabricated linear and planar colloid thruster arrays," Ph.D. dissertation, MIT, Cambridge, MA, 2004.
- [33] H. Blum, "A transformation for extracting new descriptors of shape," in *Proc. Symp. Models Perception Speech Visual Form*, W. W. Dunn, Ed., 1967, pp. 362–380.
- [34] P. E. Danielsson, "Euclidean distance mapping," *Comput. Graph. Image Process.*, vol. 14, pp. 227–248, 1980.
- [35] C.-Y. Hong and A. I. Akinwande, "Oxidation and sharpening mechanism for silicon tip formation," *Electrochem. Solid-State Lett.*, vol. 8, no. 5, pp. F13–F15, Apr. 2005.
- [36] C. Hedlund, H.-O. Blom, and S. Berg, "Microloading effect in reactive ion etching," *J. Vac. Sci. Technol. A, Vac. Surf. Films*, vol. 12, no. 4, pp. 1962–1965, Jul. 1994.
- [37] H. Jansen, M. deBoer, R. Legtenberg, and M. Elwenspoek, "The black silicon method: A universal method for determining the parameter setting of a fluorine-based reactive ion etcher in deep silicon trench etching with profile control," *J. Micromech. Microeng.*, vol. 5, no. 2, pp. 115–120, Jun. 1995.
- [38] A. H. Epstein, S. D. Senturia, O. Al-Midani, G. Anathasuresh, A. Ayon, K. Breuer, K.-S. Chen, F. E. Ehrlich, E. Esteve, L. Frechette, G. Gauba, R. Ghodssi, C. Groshenry, S. Jacobson, J. L. Kerrebrock, J. H. Lang, C.-C. Lin, A. London, J. Lopata, A. Mehra, J. O. Mur Miranda, S. Nagle, D. J. Orr, E. Piekos, M. A. Schmidt, G. Shirley, S. M. Spearing, C. S. Tan, Y.-S. Tzeng, and I. A. Waitz, "Micro-heat engines, gas turbines, and rocket engines—The MIT microengine project," presented at the 28th Fluid Dyn. Conf., Snowmass Village, CO, Jun. 29–Jul. 2, 1997, Paper AIAA-1997-1773.



**Blaise Laurent Patrick Gassend** was born in Nice, France, in 1978. He received the Dipl.Ing. degree from the École Polytechnique, Palaiseau, France, in 2001, and the M.S. degree in physical random functions and the Ph.D. degree in microfabricated electrospray thrusters arrays from the Department of Electrical Engineering and Computer Science, Massachusetts Institute of Technology, Cambridge, in 2003 and 2007, respectively.

After graduating, he was with Exponent, Inc., Menlo Park, CA, as an Associate in the Electrical and Semiconductor Practice, where he consulted on failure analysis and litigation support. Since 2009, he has been a Hardware Interface Guru at Willow Garage, Inc., Menlo Park, working on hardware and software for the PR2 robot.



**Luis Fernando Velásquez-García** (M'09) received the Mechanical Engineer degree (valedictorian of the School of Engineering, *magna cum laude*) and the Civil Engineer degree (valedictorian of the School of Engineering, *magna cum laude*) from the Universidad de Los Andes, Bogotá, Colombia, in 1998 and 1999, respectively, and the M.S. and Ph.D. degrees from the Department of Aeronautics and Astronautics, Massachusetts Institute of Technology (MIT), Cambridge, in 2001 and 2004, respectively.

In 2004, after completing his studies, he became a Postdoctoral Associate with the Microsystems Technology Laboratories (MTL), MIT, where he was appointed as a Research Scientist in 2005 and has been a Principal Scientist and Core Member since 2009. He is an expert in micro- and nanofabrication technologies, and his research focuses on the application of micro- and nanotechnologies to multiplexed scaled-down systems to attain better performance. He has conducted research in micro- and nanotechnologies applied to electrospray, carbon-nanotube-based devices, 3-D packaging, mass spectrometry, propulsion, and chemical reactors. He has authored more than 15 journal and 30 conference proceedings publications, and he is the holder of six patents on MEMS technologies.

Dr. Velásquez-García is a member of Sigma Xi.



**Akintunde Ibitayo (Tayo) Akinwande** (S'81–M'86–SM'04–F'08) received the B.Sc. degree in electrical and electronic engineering from the University of Ife, Ife, Nigeria, in 1978, and the M.S. and Ph.D. degrees in electrical engineering from Stanford University, Stanford, CA, in 1981 and 1986, respectively.

In 1986, he joined Honeywell International, Inc., Morristown, NJ, where he initially conducted research on GaAs complementary FET technology for very-high-speed and low-power signal processing. He later joined the Si Microstructures Group, where he conducted research on pressure sensors, accelerometers, and thin-film field emission and display devices. In January 1995, he joined the Microsystems Technology Laboratories and the Department of Electrical Engineering and Computer Science of The Massachusetts Institute of Technology (MIT), Cambridge, where his research focuses on microfabrication and electronic devices, with particular emphasis on smart sensors and actuators, intelligent displays, large-area electronics (macroelectronics), field emission and field ionization devices, mass spectrometry, and electric propulsion. He was a Visiting Professor in the Department of Engineering and an Overseas Fellow at Churchill College, Cambridge University, Cambridge, U.K., in 2002 and 2003. He is currently a Professor in the Department of Electrical Engineering and Computer Science, MIT. Since September 2009, he has been the Program Manager of the Microsystems Technology Office, Defense Advanced Research Projects Agency (DARPA). He is the author of more than 100 journal publications and is the holder of numerous patents in MEMS, electronics on flexible substrates, and display technologies.

Prof. Akinwande was the recipient of a 1996 National Science Foundation CAREER Award. He is currently a member of the IEEE Nanotechnology Council. He has served on a number of Technical Program Committees for various conferences, including the Device Research Conference, the IEEE International Electron Devices Meeting, the IEEE International Solid-State Circuits Conference, the International Display Research Conference, and the International Vacuum Microelectronics Conference.